Computational Structural Engineering
An International Journal
Vol. 1, No. 2, pp. 139~150 (2001)

Computational Structural Engineering Institute

Random Amplitude Variability of Seismic Ground Motions and Implications for the Physical Modeling of Spatial Coherency

A. Zerva

Department of Civil & Architectural Engineering, Drexel University, 3141 Chestnut Street, Philadelphia, PA 19104, USA

Received July 2001; Accepted November 2001

ABSTRACT

An initial approach for the identification of physical causes underlying the spatial coherency of seismic ground motions is presented. The approach relies on the observation that amplitude and phase variability of seismic data recorded over extended areas around the amplitude and phase of a common, coherent component are correlated. It suffices then to examine the physical causes for the amplitude variability in the seismic motions, in order to recognize the causes for the phase variability and, consequently, the spatial coherency. In this study, the effect of randomness in the shear wave velocity at a site on the amplitude variability of the surface motions is investigated by means of simulations. The amplitude variability of the simulated motions around the amplitude of the common component is contained within envelope functions, the shape of which suggests, on a preliminary basis, the trend of the decay of coherency with frequency.

Keywords: seismic ground motions, spatial coherency, layered site, wave propagation, simulations.

1. Introduction

The spatial variability of seismic ground motions can have a significant effect on the response of lifelines: it may induce significant additional seismic loads in the structure, than the ones induced if the motions at the structures' supports are assumed to be identical. It has been recently recognized (EERI, 1999) that the spatial variation of seismic ground motions can have a dramatic effect on the response of extended structures. Presently, in studies performed by the California Department of Transportation (Caltrans), spatially variable ground motions are used as input motions at the supports of various bridges, such as the West Bay Bridge in San Francisco and the Coronado Bridge in San Diego, California, USA (Abrahamson, 1993).

An inherent problem in incorporating the spatial variation of seismic ground motions in lifeline seismic design criteria is that it has not yet been established which spatial variability model from the extensive list that has appeared in the literature (see, e.g., Zerva & Zervas, 2002, for a review) is the most appropriate one. Generally, spatial coherency models are developed from analyses of data recorded at a single site and for a single event, and are, thus, event and site specific. Therefore, they cannot be generalized and incorporated with confidence into seismic design criteria. Attempts to fit generic models to different sites and events have not always been successful, mainly because the models are based on purely statistical measures. The statistical characterization of spatial variability results from the fact that its basic descriptor, the spatial coherency, is associated with the phase variability of the data, which is difficult to analyze and express in terms of physical quantities.

An alternative methodology for the investigation of spatially variable seismic ground motions recorded at dense instrument arrays that provides insight into physical causes affecting the seismic coherency has been developed (Zerva & Zhang, 1997). The methodology was applied to data recorded at the SMART-1 dense instrument array in Lotung, Taiwan. For each event and direction (horizontal or vertical) analyzed, the approach identifies a coherent, common component in the seismic motions recorded over extended areas. The common component represents a coherent wave train that propagates with constant velocity

† Corresponding author
Tel.: +001-215-895-2340; Fax: +001-215-895-1363
E-mail address: aspa@drexel.edu

on the ground surface and approximates to a satisfactory degree the actual motions. The spatial variability of the seismic ground motions is determined from the differences between the recorded data and the coherent estimates of the motions, and is caused by spatial arrival time delays at the array stations associated with the upward traveling of the waves through the site topography, and by variabilities in both the amplitudes and phases of the motions around the common component characteristics. It was shown that the variabilities in amplitudes and phases of the motions are correlated and, qualitatively, associated with physical parameters.

This observation sets the bases for the physical interpretation and modeling of coherency: Because amplitude and phase variability are correlated, and because amplitude variability is easier analyzed and modeled than phase variability, it suffices to examine amplitude variability and associate it with physical parameters, in order to express accordingly the phase variability, and, consequently, the spatial coherency. Analytical wave propagation schemes need then be applied to detailed models of the sites in order to quantify the causes for the amplitude and, hence, the phase variation of the motions. However, each cause needs to be isolated and examined independently of the others, so that its effect on the ground surface amplitude variability can be clearly identified. This study concentrates on local site effects, and, specifically, on the effect of random soil variability on surface ground motions. A one-dimensional model of the Lotung site is utilized. Simulations of seismic motions capturing the effect of randomness in the shear wave velocity of the layers are generated. The comparison of the amplitude variability in the simulations with that of the actual recorded data provides insight into one of the possible causes for the spatial variability in seismic ground motions. It needs to be emphasized at this point that it is by no means implied that a one-dimensional analysis captures all local site effects on the seismic ground motions, which include, among others, the dipping angle of the site, the angle of incidence of waves, two-dimensional effects etc. (see, e.g., Bard, 1994). The one-dimensional analysis is used as a first step in the identification of possible physical causes for the spatial coherency.

Section 2 of this paper provides an outline of the approach developed by Zerva and Zhang (1997), so that the continuity in the development of the methodology for the physical modeling of the spatial variability is presented and comparisons between the recorded data and the analytical results are feasible. Section 3 presents the results of the wave propagation analyses through the one-dimensional model of the Lotung site. Finally, Section 4 presents the conclusions of this work.

2. Amplitude and Phase Variability in Recorded Data

For illustration and comparison purposes, the approach developed by Zerva and Zhang (1997) is presented herein for the strong motion shear-wave window in the N-S direction of Event 5 (M_L = 6.3) recorded at the SMART-1 array in Lotung, Taiwan. At the time of the earthquake, the array consisted of 37 accelerometers arranged on three concentric circles, the inner denoted by I, the middle by M, and the outer by O with radii of 0.2, 1.0 and 2.0 km, respectively. Twelve equispaced stations, numbered 1-12, were located on each ring, and station C00 was located at the center of the array (Fig. 1). The duration of the strong motion window is 5.12 sec (7.0-12.12 sec actual time in the records) with a time step of 0.01 sec.

Initially, signal processing techniques are applied to the data for the identification of their apparent propagation characteristics. The application of the conventional method with slowness stacking to the data (Spudich & Oppenheimer, 1986) determined the slowness of the broad-band wave in the window as $\vec{s}$ ={0.1 sec/km, –0.2 sec/km}, i.e., the waves impinge the array at an azimuth of 153° with an apparent propagation velocity of 4.5 km/sec. The (horizontal) wave number, $\vec{\kappa} = (\kappa_x, \kappa_y)$, of the motions is related to the slowness through $\vec{\kappa} = \omega\vec{s}$, where ω indicates frequency in rad/sec.

The seismic motions at any location $\vec{r}$ on the ground surface are then described by the superposition of sinusoidal functions and expressed as:

$$\hat{u}(\vec{r},t) = \sum_{m=1}^{p} A_m \sin(\vec{\kappa}_m \cdot \vec{r} + \omega_m t + \phi_m) \tag{1}$$

Each sinusoidal component is described by its (discrete) frequency and wave number $(\omega_m, \vec{\kappa}_m)$; A_m and ϕ_m are its amplitude and phase shift, respectively. The amplitudes and phases, A_m and ϕ_m, of the sinusoidal components can be determined from the system of equations resulting from the least-squares minimization of the error function between the recorded time histories, $\boldsymbol{u}(\vec{r},t)$, and the approximate ones, $\hat{\boldsymbol{u}}(\vec{r},t)$ (Eq. 1), with respect to the unknowns A_m and ϕ_m (Zerva & Zhang, 1997):

$$e = \sum_{i=1}^{L}\sum_{j=1}^{N} (\boldsymbol{u}(\vec{r}_i,t_j) - \boldsymbol{u}(\vec{r}_i,t_j))^2 \tag{2}$$

evaluated at discrete locations (stations) i and times j. Any number L of stations-ranging from one to the total number of recording stations-can be used for the evaluation of the

signal amplitudes and phases. When $L>1$ in Eq. 2, the identified amplitudes and phases represent the common signal characteristics at the number of stations considered; when $L=1$, the amplitudes and phases correspond to the motions at the particular station analyzed.

Five stations ($L=5$) were initially used in Eq. 2 for the identification of their common amplitudes and phases; the stations are C00, I03, I06, I09 and I12 (Fig. 1), i.e., the center and inner stations of the array with a maximum separation distance of 400 m. Once the common characteristics are identified from the least-squares minimization of Eq. 2, they are substituted in Eq. 1, and an estimate for the motions, termed "reconstructed" motions, at the stations considered is obtained. The comparison of the recorded motions with the reconstructed ones is presented in Fig. 2. Since amplitudes and phases at each frequency are identical for all five stations considered, the reconstructed motions represent a coherent waveform that propagates with constant velocity on the ground surface. Fig. 2 indicates that the reconstructed motions reproduce to a very satisfactory degree the actual ones, and, although they consist only of the broad-band coherent body wave signal (Eq. 1), they can describe the major characteristics of the data. The details in the actual motions, that are not matched by the reconstructed ones, constitute the spatially variable nature of the motions, after the wave passage effects have been removed.

Part of the variabilities in Fig. 2 is due to the fact that the time history approximation (Eq. 1) does not allow for the small time delays in the arrival of the waves at the various stations caused by their upward traveling through the horizontal variations of the geologic structure underneath the array. Their effect can be noted in Fig. 2, when, e.g., the reconstructed motion at station I12 arrives later than the recorded one. These arrival time perturbations are partially eliminated in the approach through the alignment of the

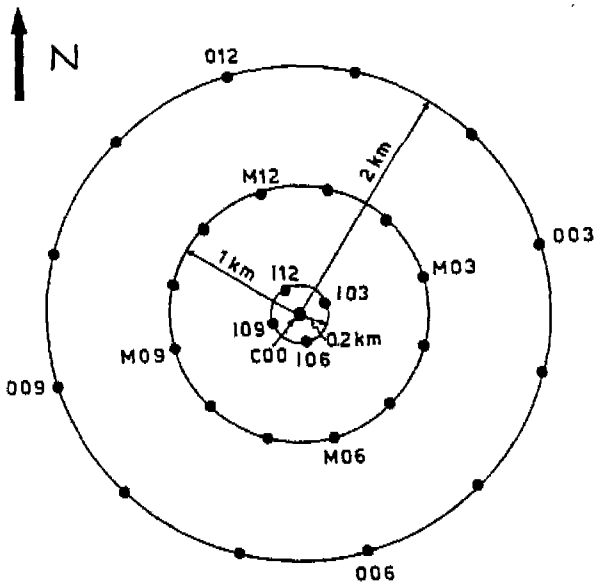

Fig. 1. The SMART-1 Array.

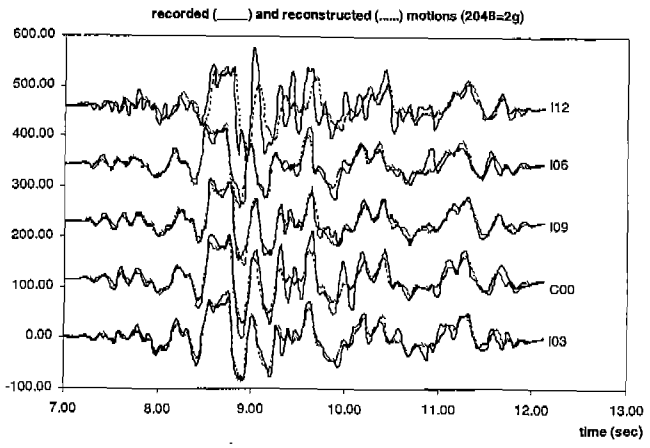

Fig. 2. Recorded and reconstructed strong shear-wave motions in the N-S direction of Event 5.

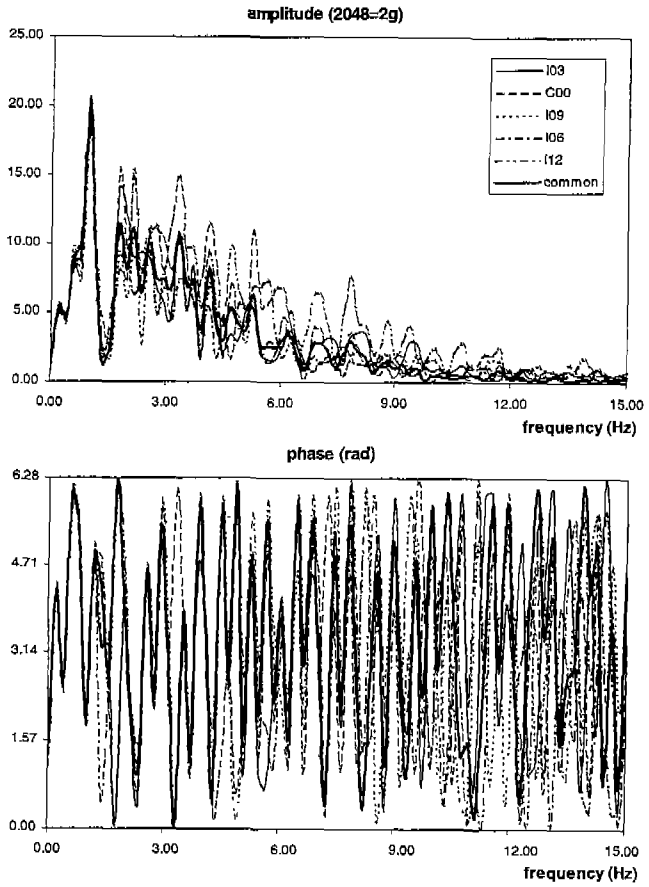

Fig. 3. Amplitude and phase variation of the aligned motions at the center and inner ring stations.

motions, which was performed with respect to the central array station, C00 (Fig. 1). An average propagation velocity evaluated from the arrival time delays of the alignment process at all stations was compatible with the constant slowness of the broad-band waves; however, the delay identified at each station exhibited a random behavior around the delay caused by the constant apparent propagation velocity across the array (Zerva & Zhang, 1997). In the following, aligned seismic ground motions are considered. For the identification of the amplitude and phase variation of the aligned motions, the error function (Eq. 2) is used again in the minimization scheme, but, in the sinusoidal approximation of the motions (Eq. 1), the term $\vec{\kappa}_m \cdot \vec{r}$ is set equal to zero, since the aligned motions arrive simultaneously at all array stations.

Fig. 3 presents the amplitude and phase variation of the sinusoidal components of the motions with frequency; the wider lines in these figures indicate the common signal characteristics, namely the contribution of the identified body wave to the motions at all five stations, whereas the thinner lines represent the corresponding amplitudes and phases when one station at a time is considered in Eq. 2. When only one station at a time (L=1 in Eq. 2) is used in the evaluation of amplitudes and phases at different frequencies for that particular station, the reconstructed motion is indistinguishable from the recorded one. This does not necessarily mean that the analyzed time histories are composed only of the identified broad-band waves, but rather that the sinusoidal functions of Eq. 1 can match the sinusoidally varying time histories, i.e., Eq. 2 becomes essentially compatible to a Fourier transform. The comparison of the results at the individual stations with the common ones (Fig. 3) provides insight into the causes for the spatial variation of the motions: In the lower frequency range (<1.5 Hz), amplitudes and phases identified at the individual stations essentially coincide with those of the common component. In the frequency range of 1.5-4.0 Hz, the common amplitude represents the average of the site amplification, and phases start deviating from the common phase. It is noted that phases were restricted in the range $[0, 2\pi)$, and, therefore, jumps of approximately 2π do not indicate drastic variation in their values. At higher frequencies, the common amplitude becomes lower than the ones identified at the stations, and phases vary randomly.

Additional analyses were performed for the middle ring stations (Zerva & Zhang, 1997). The common amplitude and phase identified from the inner and middle ring station data are remarkably similar (Fig. 4), particularly considering the facts that separate analyses were performed for the two sets of stations, and that the longest separation distance of the middle ring stations is 2 km, whereas that of the inner ring ones 400 m (Fig. 1). The agreement of the common amplitudes and phases over an extended area of 1 km radius strongly suggests the existence of the coherent component in the data. The common amplitude can be viewed as a mean value representing the average amplification of the motions at the site and is associated with the common phase that resembles random distribution between $[0, 2\pi)$ with frequency (Fig. 4). The spatial variation of the motions, in addition to their propagation effects already considered, results from deviations in both amplitudes and phases at the individual stations around the common component amplitude and phase (Fig. 2), which are described in terms of normalized differential amplitudes and differential phases presented in Fig. 5.

The normalized differential amplitudes (Fig. 5) are obtained by subtracting at each frequency the common amplitude from the amplitudes identified at the individual stations and dividing by the common amplitude. The normalized differential amplitudes are cut-off at a maximum value of 7.5; their actual values, which are not important

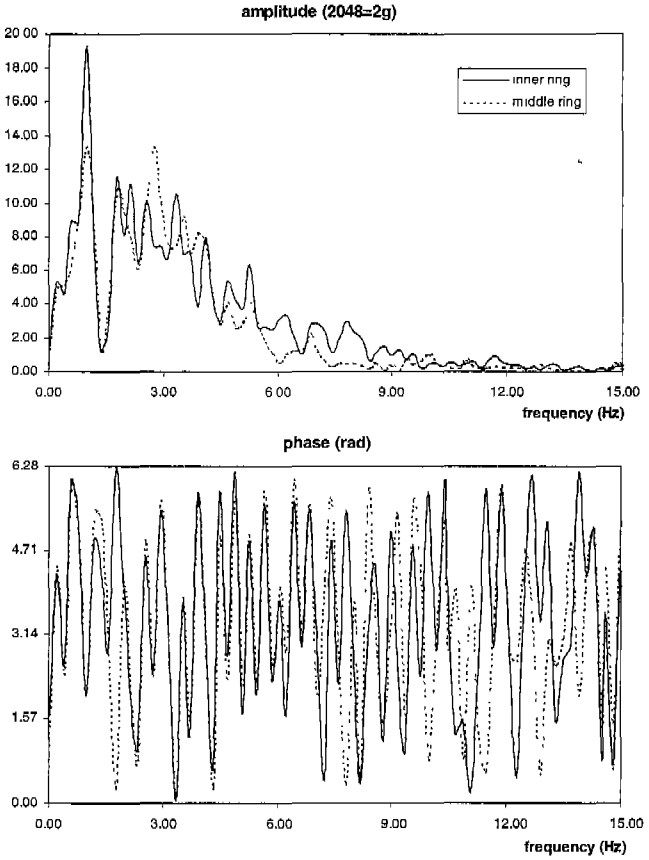

Fig. 4. Amplitude and phase variability of the inner and middle ring stations' common component.

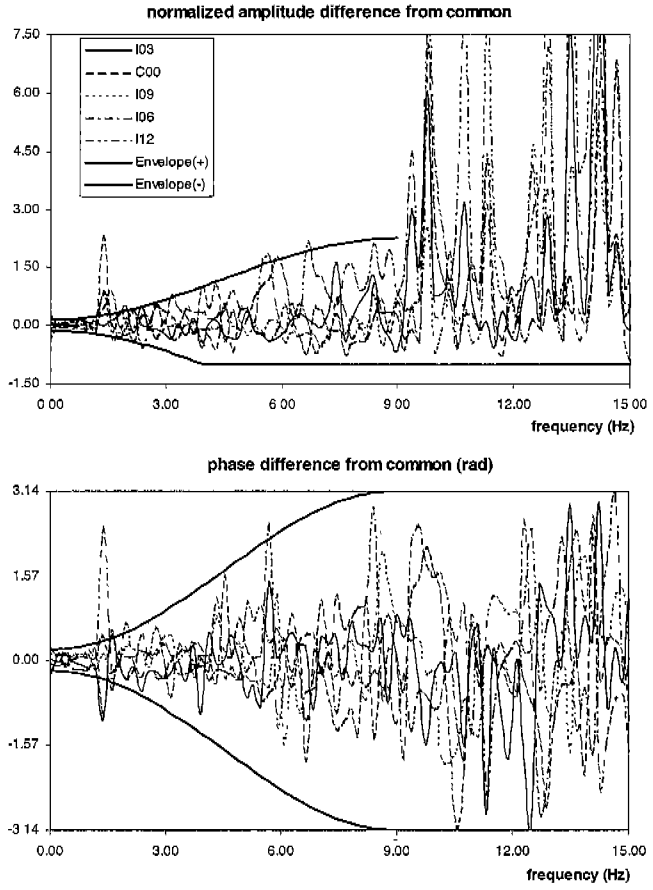

Fig. 5. Differential amplitude and phase variability of the center and inner ring stations' aligned data.

for the subsequent analysis, can be significantly high, because the common component amplitude can assume significantly low values at certain frequencies (Fig. 3). Furthermore, because of their definition, the negative values of the normalized differential amplitudes cannot become lower than (−1). The differential phases (Fig. 5) are allowed to vary between $[-\pi, +\pi)$, rather than between $[0, 2\pi)$, as was the case in Fig. 3. Envelope functions, drawn by eye, containing the amplitude and the phase differential range, are also shown in the figures. The phase envelope functions are symmetric with respect to the zero axis. Isolated peaks within the dominant site amplification frequency range are excluded from both the amplitude and phase envelope functions.

Fig. 5 indicates that the trend of the positive envelopes of both amplitudes and phases is very similar, implying that the amplitude and phase variability in the data around their respective common component characteristics are correlated. This observation allows the possibility of the physical interpretation and modeling of the phase variability in the seismic data, and, subsequently, the spatial coherency. Phase variability is difficult to visualize and attribute to physical causes. On the other hand, the causes for the amplitude variability are easier visualized and examined. If the variability of amplitudes and phases in the seismic data are correlated, as the present analysis indicates, it suffices to examine the physical causes for the amplitude variability in the seismic motions, in order to recognize physical causes underlying the phase variability. Indeed, the variability in amplitudes and, due to their correlation, in phases presented in Fig. 5 can be qualitatively-associated with physical parameters: In the low frequency range, the envelope functions for both amplitudes and phases are at close distance to the zero axis; this is attributed to the long wavelength of the contributing waves at low frequencies, that do not "see" the site irregularities particularly for the relatively close-by stations of the inner ring. As frequency increases within the dominant site amplification frequency range, the distance of the amplitude and phase envelope functions from the zero axis increases gradually. In this range, the common amplitudes reproduce the average of the site amplification (Fig. 3), implying that the motions are controlled by the broad-band wave that is modified in amplitude and phase as it traverses the horizontal variations of the layers underneath the array. The increase in the variabilities of amplitudes and phases around the common component as frequency increases may also be associated with the decreasing wavelength of the waves at increasing frequencies, and to the more significant contribution of scattered energy. At higher frequencies, past the dominant site amplification frequency range, wave components in addition to the broad-band shear wave, and, mainly, scattered energy (noise) dominate the motions. Because these wave components propagate at different velocities, phases at individual stations (Fig. 3) deviate significantly from the common phase, and the common signal amplitude no longer represents the average of the site amplification and becomes lower than the amplitudes identified at the individual stations. Consequently, the phase differences vary randomly between $(-\pi, +\pi)$, i.e., the differential phase envelopes are parallel to the zero axis at a distance equal to π, and the normalized differential amplitudes assume high values. Noise is also the cause of the isolated peaks in the dominant frequency range of the motions: it occurs when amplitudes are low within the dominant frequency range of the motions (Fig. 3). Similar qualitative correlations in the amplitude and phase variation of the motions around the common component amplitude and phase have been observed from the analysis of the middle ring station data (Zerva & Zhang, 1997). In this case, however, the distance

of the envelope functions for both amplitudes and phases at lower frequencies is longer than that of the inner ring stations, and the frequency range before differential phases vary randomly between $(-\pi, +\pi)$ and normalized differential amplitudes assume high values is shorter than that of the inner ring stations; both observations are an expected consequence of the longer separation distance between the middle ring stations (Fig. 1).

The envelope functions in Fig. 5 contain the variability range of amplitudes and phases with respect to the common component for motions recorded at separation distances less than the maximum separation distance for the area considered. Thus, the envelope functions, as upper limits, are functions of frequency and maximum station separation distance, i.e., 400 m for the inner ring data. Constrained within the envelope functions, differential amplitudes and phases vary randomly, suggesting that the variability can be described by the product of the envelope function and a random number uniformly distributed within a specific range. Differential amplitudes and phases between the motions at different stations - rather than between the motion at each station and the common component - also vary randomly within bounds of envelope functions, that have trends very similar to those of the envelope functions with respect to the common component, an observation that can be readily made from Fig. 5. Differences in phases between stations are directly related to coherency through envelope functions containing their random variability.

Abrahamson (1992) established the relation between phase variability and coherency, which is summarized in the following: Let $\phi_j(\omega)$ and $\phi_k(\omega)$ be the phases at two recording stations j and k on the ground surface, after the wave passage effects have been removed. The relation between $\phi_j(\omega)$ and $\phi_k(\omega)$ can be expressed as:

$$\phi_j(\omega) - \phi_k(\omega) = \beta_{jk}(\omega)\pi\varepsilon_{jk}(\omega) \tag{3}$$

in which, $\varepsilon_{jk}(\omega)$ are random numbers uniformly distributed between $[-1, +1]$, and $\beta_{jk}(\omega)$ is a deterministic function of frequency and assumes values between 0 and 1. $\beta_{jk}(\omega)$ indicates the fraction of the random phase variability between $[-\pi, +\pi)$ that is present in the phase differences of the motions between the two stations. For example, if $\beta_{jk}(\omega) = 0$, there is no phase difference between the two stations, and the phases are identical and fully deterministic. In the other extreme case, i.e., when $\beta_{jk}(\omega) = 1$, the phase difference of the motions between stations is completely random. Based on Eq. 3 and neglecting the amplitude variability in the data Abrahamson (1992) noted that the mean value of the coherency, $\gamma_{jk}(\omega)$, after propagation effects have been removed, can be expressed as:

$$E[\gamma_{jk}(\omega)] = \frac{\sin(\beta_{jk}(\omega)\pi)}{\beta_{jk}(\omega)\pi} \tag{4}$$

It is easy to verify from Eq. 4 that when the coherency tends to one, $\beta_{jk}(\omega)$ is a small number, i.e., only a small fraction of randomness appears in the phase difference between the motions at the two stations; as coherency decreases, $\beta_{jk}(\omega)$ increases, and, for zero coherency, $\beta_{jk}(\omega) = 1$.

Equations 3 and 4 and Fig. 5 then indicate that the differential phase variability identified by means of the present methodology is equivalent to conventional coherency estimates. However, the developed approach recognizes that the shape of the envelope functions, and, consequently, the associated coherency is related to physical parameters: In the low frequency range, where the envelope functions are close to the zero axis, coherency assumes values close to one; this behavior follows from the phase differences in the low frequency range and is a consequence of the signal wavelength. Within the dominant site amplification frequency range of the motions, where the envelope functions increase with frequency, coherency decreases; this may be attributed to the dominance of the body wave in the records, to the decreasing wavelength of the motions, and to the more significant contribution of scattered energy. In the higher frequency range, where phases vary randomly between $[-\pi, +\pi)$ and noise dominates, coherency assumes zero values.

Table 1. Soil Properties of Lotung Site

Layer	H	ρ	V_S	$(\text{c.o.v.})_{V_S}$	ξ
	(m)	(kg/m^3)	(m/sec)	%	%
1	1.2	1900.0	60.0	24.74	5.0
2	1.8	2000.0	75.0	25.66	6.0
3	4.5	1980.0	100.0	12.08	6.0
4	4.5	1900.0	90.0	9.12	6.0
5	6.0	1950.0	100.0	10.50	6.0
6	10.0	2130.0	150.0	8.75	6.0
7	14.0	1870.0	130.0	8.88	6.0
8	18.0	1830.0	140.0	5.97	6.0
9	60.0	1900.0	400.0	5.63	1.0
10	80.0	2000.0	850.0	6.04	0.5
half space	∞	2000.0	1700.0	6.79	0.5

3. Seismic Ground Motion Simulations Through Stochastic Layers

The identification of the correlation patterns of amplitude and phase variability in the recorded motions around the common, coherent component sets the basis for the physical modeling of coherency. As a first approach in quantifying physical parameters affecting coherency, this study analyzes the effect of randomness in the shear wave velocity of the layers of a site on the surface motion amplitude variability. For this purpose, a model of the soil profile at the Lotung site (Wong & Luco, 1990) is utilized. It is considered that the site can be approximated by ten horizontal layers overlying the bedrock (half space). One-dimensional wave propagation analysis is considered, and Monte Carlo simulations are performed to capture the effect of randomness in the shear wave velocity of the layers on the ground surface amplitude variability.

Wong and Luco (1990) presented a detailed examination of the soil properties at the Lotung site. Based on geotechnical and geophysical information, they derived a set of models for the site, including possible variabilities in the soil characteristics over short distances. Their soil models were used to blindly predict the response of a containment model built at the site. In the following, their high-strain model based on soil data and geophysical information is used. This model is selected because: (i) it is based on basic soil mechanics data and geophysical information; and (ii) the high-strain model corresponds to an equivalent linear model for strains compatible with free-field ground motions characterized by peak ground acceleration of 0.2 g, consistent with Event 5 (peak ground acceleration of 0.24 g). It is emphasized at this point that the information for the soil profile is restricted over a relatively small area (50×100 m), surrounding the containment model; more significant variability in the soil characteristics and profile ought to be expected at longer distances. Table 1 presents the soil model characteristics used in the present analysis. The site consists of 10 horizontal layers with a total depth of 200 m overlying the half space. The height, H, density, ρ, mean value of the shear wave velocity, V_S, with its associated coefficient of variation, $(\text{c.o.v})_{V_S}$, and damping coefficient, ξ, of each layer are also presented in the table.

One-dimensional shear wave propagation analyses (Aki & Richards, 1980) on the model of the site are performed. The analyses consider vertical incidence of an impulse function at the interface between the half space and the layers. Accordingly, the resulting motions on the ground surface represent the impulse response functions of the site. It is also considered that, within each layer, the shear wave velocity varies randomly, according to a uniform distribution with mean and c.o.v. as presented in Table 1. In order to identify the effects of the variability of each layer on the resulting seismic ground motions, the characteristics of all layers (including the half space) except one at a time were considered deterministic and equal to their mean value. Simulations are then performed by allowing the shear wave velocity of one layer at a time to vary randomly. In the last case, it is considered that the shear wave velocity of all layers as well as the half space vary randomly within their specified bounds. Once the simulations for each case are obtained, the "common" component of the simulations is identified and its amplitude evaluated. Normalized differential amplitudes are obtained from the amplitude of each simulation and the common component amplitude. Envelope functions containing the variation of the amplitude of the simulations around the common component amplitude are then determined, so that the effect of randomness in the shear wave velocity at the site on the resulting surface motions is identified.

Fig. 6 presents the common component amplitude evaluated from the simulations that allowed random variability in the shear wave velocity of all layers. For comparison, the amplitude of a deterministic wave propagation analysis utilizing the mean value of the shear wave velocity in each layer (Table 1) is also presented. The amplitudes are normalized with respect to the maximum value of the "deterministic mean" amplitude. The shape of the response functions in both cases is similar, except for the fact that the common component is "smoother" than the "deterministic mean". For all simulations performed, the result-

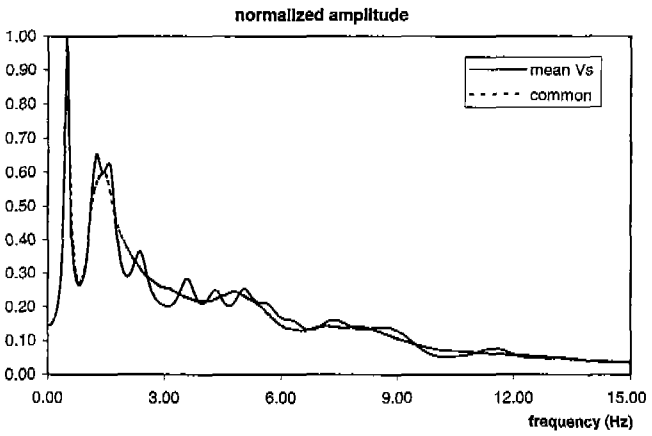

Fig. 6. Normalized amplitude of the analytically evaluated common component and the deterministic analysis using the mean value of the shear wave velocity profile.

ing site response functions showed similarity in shape; the differences, however, between the smoother common component and the more variable simulations identify the causes for the spatial variability of the motions, as was also the case in the comparison between the common amplitude and the amplitudes identified at the individual stations of the SMART-1 array (Fig. 3).

The comparison of the analytical common component amplitude (Fig. 6) with the common component amplitude obtained from the recorded data (Fig. 4) shows similarities between the data and the analytical results: Both figures indicate a sharp peak at the low frequencies, though the one for the analytical results has a shorter bandwidth; this may be attributed to the estimated damping coefficients for the high-strain model developed for the site. Also, Fig. 6 suggests that the dominant frequency range of the motions (Fig. 4) is captured by the analytical model, though the decay of amplification is more prominent in the analytical results. The differences in Figs. 4 and 6 should be expected: As has been already indicated, a one-dimensional wave propagation scheme can not fully represent the actual site geometry and wave incidence, that have been shown to affect seismic motions on the free surface of a sediment site (e.g., Bard, 1994). Furthermore, the analytical results are actually impulse response functions, whereas the actual data contain information about source, source-site and local site effects. It is, however, noted that, in this initial approach for estimating causes underlying the amplitude variability in the seismic motions, the analytical results present a reasonable approximation of the site response characteristics; the approach is, also, a simple, quantitative way to identify the degree to which variability in the characteristics of the site affects the surface ground motions.

Envelope functions containing the variability of the normalized differential amplitudes for representative layers are shown in Figs. 7-10. Fig. 7 presents the envelope functions for random variability in the shear wave velocity of the top two layers, Fig. 8 the corresponding results for random variability in the third and sixth layers, Fig. 9 the ones for random variability in the eighth and ninth, and, finally, Fig. 10 presents the case of random variability in the shear wave velocity of the half space and the case where the shear wave velocity varies randomly in all layers. In all cases, the envelope functions are essentially symmetric around the zero axis, and their absolute values do not exceed unity. It is noted that the positive normalized differential amplitude variability obtained from the recorded data assumes significantly high values at higher frequencies (Fig. 5). This difference, however, between the

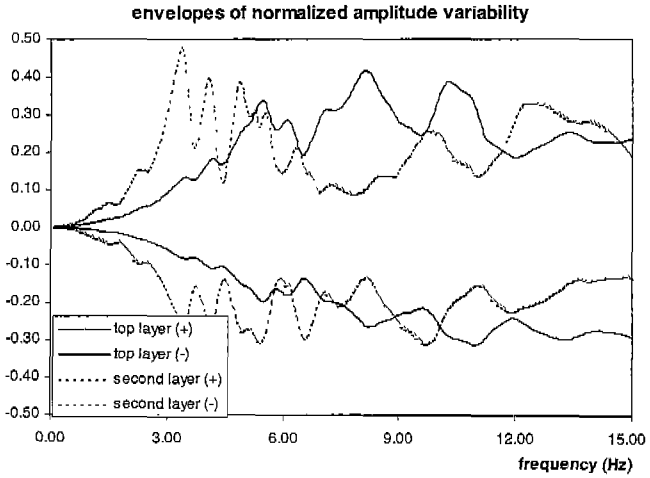

Fig. 7. Effect of the randomness in shear wave velocity of the top and second layers on the surface motion amplitude.

analytical results and the actual data is expected: The simulations contain only the broad-band wave; hence, the common component of the analytical results will always represent an "average" of the simulations. On the other hand, the recorded data contain additional wave components, including scattered energy/noise, the presence of which dominates as frequency increases, and is the cause for the large amplitude variability in Fig. 5.

When the shear wave velocity of a layer varies, the peaks and valleys of the resulting surface amplitudes are shifted and their amplitudes change, so that the values of the normalized differential amplitudes become high close to the peaks and valleys of the site's response (Fig. 6). Fig. 7-10 reflect this pattern and, in particular, indicate the frequency range where the variability in the shear wave velocity of the individual layers has a significant effect on the resulting surface motions. Fig. 7 indicates that, although the top layer is very thin (1.2 m), it has a significant effect on the amplitude variability of the surface motions; this is associated with the fact that its c.o.v. is quite large (Table 1), as should be the case for the top layers of a site. The envelope function for the normalized differential amplitude variability for this layer increases with frequency; this may be attributed to the decreasing wavelength of the motions as frequency increases, so that the layer becomes more "obvious" to the incoming waves at higher frequencies. A similar pattern is observed for variability in the shear wave velocity of the second layer (Fig. 7); this layer is also thin (1.8 m) with a large c.o.v. (Table 1). The layer does also not affect the very low frequency range of the motions; however, in this case, large amplitude variability is observed from approximately 3 Hz and above, i.e., from frequencies that are lower than those of

the first layer. It is noted that randomness in the shear wave velocity in these two top layers produces the highest amplitude variations than in any other layer (Figs. 7-10). For the third layer (Fig. 8), variability in amplitudes starts in the low frequency range, is significant in the range from 3-8 Hz, and remains small as frequency increases past 8 Hz. Randomness in the shear wave velocity of layers below the third one resulted in a similar pattern for the amplitude variability; another example of the pattern is the amplitude variability caused by random shear wave velocity in the sixth layer, which is also depicted in Fig. 8. It is noted from Fig. 8 that the maximum amplitude of the envelope functions decreases as the depth of the layers from the ground surface increases. However, the distance of the envelope functions from the zero axis in the very low frequency range (<1 Hz) is longer for random shear wave velocity in the sixth layer than in the third (Fig. 8); the same observation can also be made for the amplitude variability due to random shear wave velocity in the fourth and fifth layer (not shown herein). This increase in the low frequency range is again noted in the amplitude variations for randomness in the shear wave velocity of the eighth layer (Fig. 9)-and, also, for the seventh (not shown herein). At first glance, it may appear that the small decrease in the values of the shear wave velocities of the fourth, seventh and eighth layers as compared to their surrounding ones (Table 1) is the cause for this increase. To examine this assumption, additional analyses have been performed for a more simple Lotung site model, where the layers one and two were combined to a single one, layers three, four and five to a second, and layers six, seven and eight to a third; the velocity of the combined layers was equal to the average of the original ones (Table 1), and no shear wave velocity reduction occurred with depth. Still, a similar pattern was observed, particularly for the layer that contained the original sixth, seventh and eighth ones (Table 1). The most probable cause for this behaviour is that the randomness in the shear wave velocity of these layers affects the amplitude and location of the first, dominant peak of the site response (Fig. 6), and a small change in this high peak causes large amplitude variabilities. For random shear wave velocity in the ninth layer (Fig. 9) significant amplitude variability is observed in the higher frequency range. This may be attributed to the characteristics of the layer (Table 1): it is the first layer with a dramatic change in shear wave velocity, damping and depth, associated with a significant shear wave velocity c.o.v. A similar, but much less dramatic, behavior is observed in the simulations for random shear wave velocity of the tenth layer. Random variability in the half space shear wave velocity produces, essentially, the lowest amplitude variability in the surface motions (Fig. 10). Fig. 10 also presents the envelope functions for the simulations when random shear wave velocity in all layers including the half space is considered. The resulting envelope functions for the latter case show significant amplitude variability throughout the entire frequency range, that is associated with the much more significant shifts in frequency and change in amplitude of the peaks and valleys of the site's response (Fig. 6).

An interesting observation can be made regarding the amplitude variability obtained from the envelopes of the simulated motions (Figs. 7-10) in comparison to the one obtained from the actual data (Fig. 5). The envelopes of normalized differential amplitude variability when random shear wave velocity in one layer at a time is considered are fairly consistent with the normalized amplitude variability

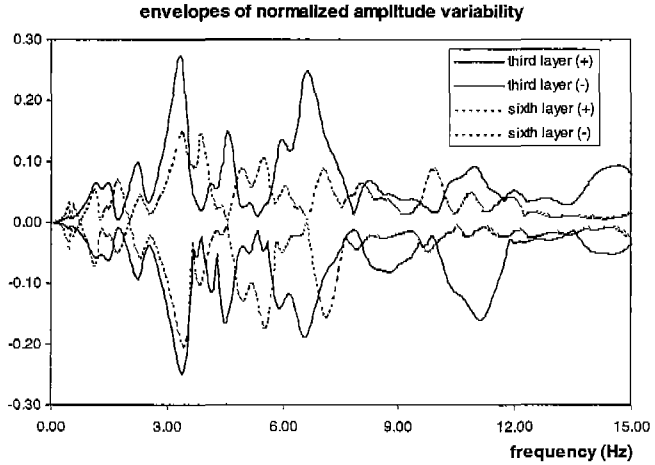

Fig. 8. Effect of the randomness in shear wave velocity of the third and sixth layers on the surface motion amplitude.

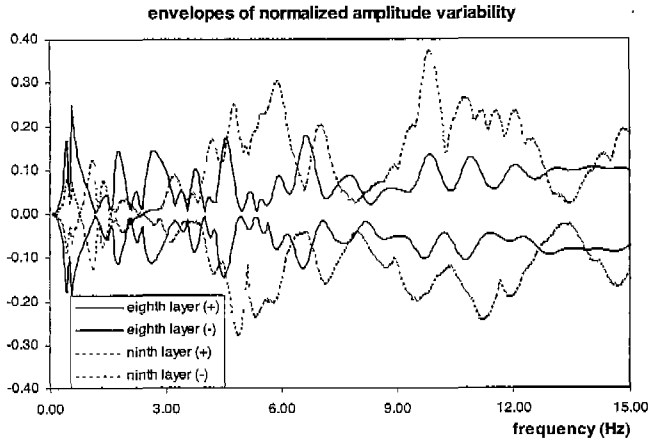

Fig. 9. Effect of the randomness in shear wave velocity of the eighth and ninth layers on the surface motion amplitude.

of the recorded data. The consistency is, of course, conditional on the fact that the actual motions contain components in addition to the broad-band wave, that dominate as frequency increases and cause the large positive normalized differential amplitude variability in Fig. 5. Another difference between the amplitude envelope functions of the analytical results and the recorded data is the high peak in the low frequency range (<1 Hz) that is observed in Fig. 9. As already indicated, this peak in the envelope functions is associated with the first dominant frequency of the analytical motions, that is lower than that of the actual ones (Figs. 3 and 6). The value of this peak in the amplitude envelope functions is significantly amplified when randomness in the shear wave velocity of all layers is considered (Fig. 10); its value actually exceeds the value of the amplitude envelope function obtained from the recorded data (Fig. 5): The envelope functions for the

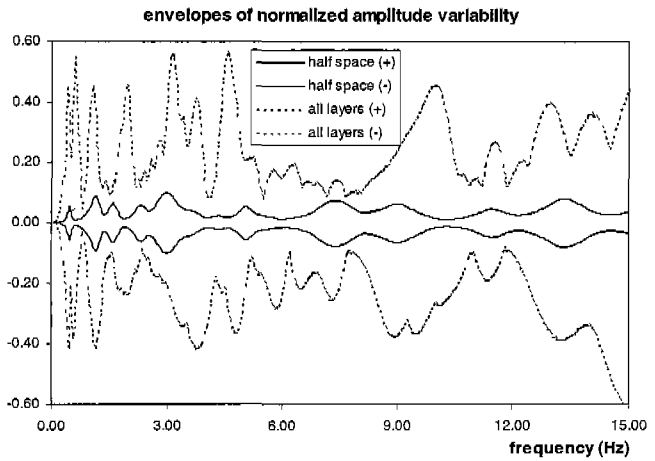

Fig. 10. Effect of the randomness in shear wave velocity of the half space and all layers on the surface motion amplitude.

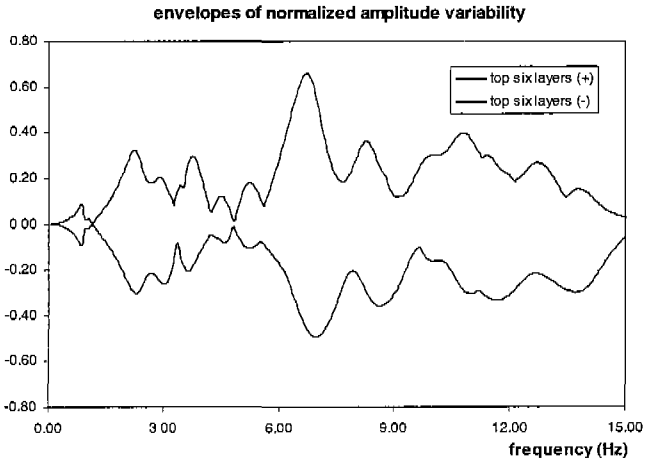

Fig. 11. Effect of the randomness in shear wave velocity of the top six layers of the site on the surface motion amplitude.

actual data assume values (–0.2, +0.2), (–0.4,+0.4), and (–0.7, +0.7) at, approximately, 1 Hz, 2 Hz, and 3 Hz, respectively (Fig. 5). The envelope functions of the simulated motions with random shear wave velocity in all layers reach values past the range (–0.5, +0.5) at frequencies below 1 Hz. This may be an artifact of the high-strain Lotung site model that considers significantly low values of damping, but it also implies that the consideration of random variability in the shear wave velocity of all layers may be excessive. Indeed, Anderson *et al.* (1996), suggested that, if a site can be sufficiently well approximated by a one-dimensional model, the first 30 m control the response; in the present case, this implies layers one to six (total depth of 28 m).

Fig. 11 presents the envelope functions of the simulations generated with the consideration that the shear wave velocity of the top six layers (Table 1) varies randomly. Although it is by no means implied that the results of a one-dimensional wave propagation analysis with random shear wave velocity in the top layers (Fig. 11) would capture the amplitude variability of actual recorded data (Fig. 5), the comparisons of Figs. 5, 10 and 11 suggests that random shear wave velocity in the top 28m of the array (Fig. 11) produces envelope functions for the normalized amplitude variability more consistent with that of the recorded data (Fig. 5), than when random shear wave variability in all layers is considered (Fig. 10). As already indicated in the previous section, the variation of the amplitude variability of seismic ground motions around the amplitude of the common component is correlated with the phase variability around the common phase; the phase variability is then related to the coherency (Eqs. 3 and 4). For illustration purposes only, Fig. 12 presents an estimate for the spatial coherency, if randomness in the shear wave velocity of the six top layers of the site is considered. It is noted that Fig. 12 represents the coherency of seismic motions with respect to the common component, rather than between two different simulations, as would be the conventional definition of coherency. The coherency plot in Fig. 12 was obtained from the envelope function of Fig. 11 and Eq. 4, with the assumption that the peak of the envelope function in Fig. 11 corresponds to the maximum value of the phase (i.e., π). Since the soil variability in the data provided by Wong & Luco is valid for an area of 50 ×100 m, the coherency estimate in the figure is valid up to the maximum separation distance between points in the area, namely its diagonal (111.8 m). The illustration of the analytical coherency in Fig. 12 indicates that its value drops when the value of the amplitude envelope increases (Fig. 11), and, accordingly, becomes smallest at the peak

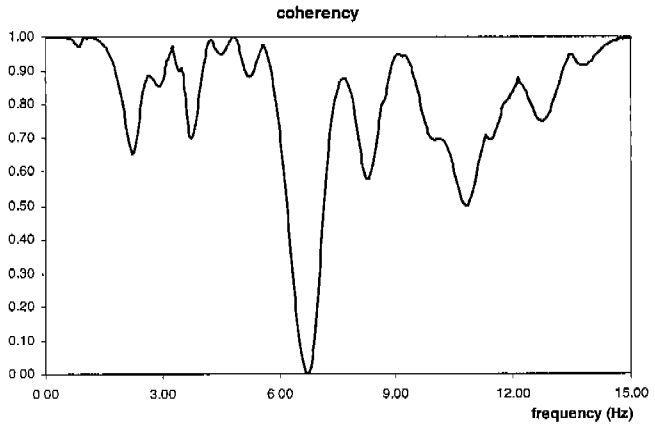

Fig. 12. Estimate for the spatial coherency based on the randomness in the shear wave velocity of the top six layers of the site for maximum separation distance of 111.80 m.

of the envelope function. At high frequencies, the illustrative coherency increases, as expected: since the simulations contain only the broad-band wave, seismic motions are correlated even at high frequencies. It needs to be emphasized at this point that the coherency presented in Fig. 12 is by no means intended as a "site-specific" coherency; it is presented as an illustration of the possibility of the approach. Additional causes for the amplitude variation of the motions need to be fully analyzed before a conclusive site-specific coherency estimate is obtained.

4. Summary and Conclusions

Coherency is a measure of the correlation of seismic motions over extended areas. It is obtained from regression analyses of data with large scatter, and represents the phase variability in recorded seismic motions; as such, its analytical modeling becomes difficult. An alternative methodology for the investigation of spatially variable ground motions has been developed (Zerva & Zhang, 1997). The approach identifies a common, coherent component in seismic motions recorded over extended areas for each event, direction and time window analyzed. The spatial variation of the motions is then determined from the differences between the recorded data and the coherent estimates of the motions. The application of the approach to data recorded at the SMART-1 array in Lotung, Taiwan, revealed that the variabilities in the amplitudes and phases of the motions recorded at individual stations around the common component characteristics are correlated. This observation sets bases for the physical interpretation and, eventually, modeling of coherency: Because the deviations of amplitudes and phases around the common component are correlated, it suffices to examine amplitude variability and attribute it to physical causes, in order to express accordingly the phase variability and, consequently, the spatial coherency.

This study presents the first effort in quantifying one possible cause for the amplitude variability of the motions on the surface of the SMART-1 site. It concentrates on local site effects and, specifically, on the investigation of the effects of randomness in the shear wave velocity of horizontal layers on the amplitude variation of surface motions. A one-dimensional wave propagation scheme with vertical incidence of shear waves is utilized in simulations. The simulated motions capture the effect of variability in the shear wave velocity of one layer at a time, as well as variability in all layers including the half space. It is found that, although the top two layers at the site are thin, their contribution to the amplitude variability is significant over the entire frequency range. The lowest amplitude variability, for the site under consideration, is caused by the variability in the shear wave velocity of the half space. The intermediate layers produce similar amplitude variability, dependent on the c.o.v. of their shear wave velocity, and consistent with the fact that a change in shear wave velocity causes a shift in the frequency location and change in the amplitude of peaks and valleys of the site's response. It is also found that the consideration of random variability in all layers can be excessive: The amplitude variability in the simulations exceeds that of the recorded data. On the other hand, the variability in the shear wave velocity of the top (in the present case, six) layers produces results consistent with those of the recorded data for the site under consideration and under the limitations of a one-dimensional model. As an illustration of the approach a possible estimate of the coherency based on the randomness in the shear wave velocity of the site's top six layers is also presented. The present analysis indicates that, when all causes for the amplitude variation of the seismic ground motions have been considered and the significant ones identified, a "site-specific" coherency estimate can be feasible; analyses towards this goal are presently under way.

Acknowledgements

This study was supported by the USA National Science Foundation (NSF) under Grants CMS-9725567 and CMS-9870509.

References

Abrahamson NA (1992) Generation of spatially incoherent strong motion time histories, Proc. 10th World Conf. Earthq. Eng.,